Three-Wave Backward Optical Solitons

Carlos Montes, Pierre Aschieri, Antonio Picozzi, C. Durniak, Majid Taki

Three-Wave Backward Optical Solitons

Carlos Montes[1,*], Pierre Aschieri[1], Antonio Picozzi[2], Céline Durniak[3], and Majid Taki[3]
[1]*CNRS, Laboratoire de Physique de la Matière Condensée, Université de Nice - Sophia Antipolis, F-06108 Nice Cedex 2, France*
[2]*CNRS, Institut Carnot de Bourgogne, F-21078 Dijon Cedex, France*
[3]*Laboratoire de Physique des Lasers, Atomes et Molecules, Université des Sciences et Technologies de Lille, F-59655 Villeneuve d'Asq Cedex, France*
[*]*Corresponding author: carlos.montes@unice.fr*

Abstract

Three-wave solitons backward propagating with respect to a pump wave are generated in nonlinear optical media through stimulated Brillouin scattering (SBS) in optical fibers or through the non-degenerate three-wave interaction in quadratic ($\chi^{(2)}$) nonlinear media. In an optical fiber-ring cavity, nanosecond solitary wave morphogenesis takes place when it is pumped with a continuous wave (c.w.). A backward dissipative Stokes soliton is generated from the hypersound waves stimulated by electrostriction between the forward pump wave and the counterpropagating Stokes wave. Superluminous and subluminous dissipative solitons are controlled via a single parameter: the feedback or reinjection for a given pump intensity or the pump intensity for a given feedback. In a c.w. pumped optical parametric oscillator (OPO), backward picosecond soliton generation takes place for non-degenerate three-wave interaction in the quadratic medium. The resonant condition is automatically satisfied in stimulated Brillouin backscattering when the fiber-ring laser contains a large number of longitudinal modes beneath the Brillouin gain curve. However, in order to achieve quasi-phase matching between the three optical waves (the forward pump wave and the backward signal and idler waves) in the $\chi^{(2)}$ medium, the nonlinear susceptibility should be periodically structurated by an inversion grating of sub-μm period in an optical parametric oscillator (OPO). The stability analysis of the inhomogeneous stationary solutions presents a Hopf bifurcation with a single control parameter which gives rise to temporal modulation and then to backward three-wave solitons. Above OPO threshold, the nonlinear dynamics yields self-structuration of a backward symbiotic solitary wave, which is stable for a finite temporal walk-off, i.e. different group velocities, between the backward propagating signal and idler waves.

We also study the dynamics of singly backward mirrorless OPO (BMOPO) pumped by a broad bandwidth field and also with a highly incoherent pump, in line with the recent experimental demonstration of this BMOPO configuration in a KTP crystal. We show that this system is characterized, as a general rule, by the generation of a highly coherent backward field, despite the high degree of incoherence of the pump field. This remarkable property finds its origin in the convection-induced phase-locking mechanism that originates in the counter-streaming configuration: the incoherence of the pump is transferred to the co-moving field, which thus allows the backward field to evolve towards a highly coherent state.
We propose other realistic experimental conditions that may be implemented with currently available technology and in which backward coherent wave generation from incoherent excitation may be observed and studied.

1 Introduction

In nonlinear wave systems, resonance processes may give rise to solitary waves resulting from energy exchanges between dispersionless waves of different velocities. Three-wave resonant interaction in nonlinear optical systems [1], plasmas [2] [3] and gases [4] predict symbiotic three-wave solitary waves in analogy to self-induced transparency [5] [6]. The structure of them is determined by a balance between the energy exchanges rates and the velocity mismatch between the three interacting waves. The three-wave interaction problem has been the object of many theoretical studies and numerical simulations as we referred in Refs. [7] [8]. The non-conservative problem in the presence of a continuous pump has been integrated by the inverse scattering transform (IST) in the non-dissipative case [6], giving rise to backscattered solitons. Our interest has been to study this non-conservative problem in the presence of dissipation or cavity losses, because this kind of backward structuration has been experimentally obtained in stimulated Brillouin scattering of a c.w. pump wave into a backward red-shifted Stokes wave in long fiber-ring cavities. It has been shown in a Brillouin fiber-ring cavity that, spontaneous structuration of dissipative three-wave solitary waves takes place when the source is a c.w. pump [9, 10, 11, 12]. The periodic round-trip interaction in a long lossy cavity may be associated to the non-conservative unlimited interaction [8] [11]. The nonlinear space-time three-wave resonant model between the two optical waves and the dissipative material acoustic wave satisfactorily explains the generation and the dynamics of the backward-traveling solitary pulses in the fiber-ring cavities. Stability analysis of the inhomogeneous stationary Brillouin mirror solution in the c.w.-pumped cavity [10] exhibits a one-parameter Hopf bifurcation. Below a critical feedback, a time-dependent oscillatory regime occurs, and self-organization of a localized pulsed regime takes place. Experimental results and dynamical simulations confirm this scenario. A stable continuous family of super-luminous and sub-luminous backward-traveling dissipative solitary pulses is obtained through a single control parameter [11] [12]. A parallel analysis in an unbounded one-dimensional medium shows that the integrable three-wave super-luminous symmetrical soliton is unstable for small dissipation, and that it cascades to a turbulent multi-peak structure. The general non-symmetrical and non-integrable case is dependent only on the exponential slope of the wave front of the backscattered Stokes wave, thus providing the stable super- and sub-luminous dissipative solitary attractors [8]. An overview of the experimental results for a large set of input pump powers and Stokes feedback conditions shows a remarkable agreement with the numerical simulations of the three-wave coherent partial differential equations model [12]. We will not consider this topic here and refer the reader to a recent review article [13] where this kind of dissipative soliton has been discussed in details.

This review article is devoted to the resonant interaction of three optical waves (called pump, signal and idler) in a nonlinear quadratic material. The same mechanism, responsible for nanosecond solitary wave morphogenesis in the Brillouin-fiber-ring laser may act for picosecond backward pulse generation in a quasi-phase matched (QPM) optical parametric oscillator (OPO) [14, 15, 16, 17, 18, 19]. The dissipative character will rise from the partial reinjection of one wave (in the singly resonant OPO), two waves (in the doubly resonant OPO) or to the absorption losses in a backward mirrorless OPO. The resonant condition for the wavevectors is automatically satisfied in stimulated Brillouin backscattering when the fiber ring laser contains a large number of longitudinal modes beneath the Brillouin gain curve. However, in order to achieve counter-streaming QPM matching between the three optical waves in the $\chi^{(2)}$ medium, a nonlinear susceptibility inversion grating of sub-μm period is required [20, 21, 22, 23]. In the non-degenerate three-wave case of a backward quasi-phase matching configuration in the quadratic media where both signal and idler fields propagate backward with respect to the direction of the pump field, the first order quasi-phase-matching pitch is of order $\lambda_p/2n_p$ where n_p is the refractive index at the pump wavelength λ_p. This can be achieved for example by periodic poling techniques but up to now the polarization inverted grating of sub-μm period has been only obtained for the backward idler configuration in a $KTiOPO_4$ crystal which allows the realization of a mirrorless optical parametric oscillator (MOPO) [24] with remarkable spectral properties [25, 26]. Therefore, higher-order Bragg condition have been suggested [22]. However, the interest of the first order configuration is that the solitary waves can be spontaneously generated from noise by a c.w. pump when the quadratic material is placed inside a singly resonant OPO (where singly stands here for only one wave reinjection).

Parametric interaction of counter-propagating signal and idler waves has the unique property of automatically establishing distributed feedback without external mirrors and thus realizing sources of coherent and tunable radiation. A recent experimental demonstration of such a mirrorless optical parametric oscillator (MOPO) has been performed in a 800 nm periodically poled $KTiOPO_4$ (PPKTP) configuration [24] with a pulse pump. The forward oscillator signal is essentially a wavelenght-shifted replica of the pump spectrum, and the backward generated idler pulse has a bandwidth of two orders of magnitude narrower than that of the pump [25, 26]. This sub-μm periodic configuration where QPM is achieved with a pump and signal waves propagating in the forward direction and the idler wave in the backward direction [*cf.* 1(b)] opens the way for achieving the shorter periodicity required for a QPM configuration where both signal and idler backward propagate with respect to the pump wave [*cf.* 1(d)]. As we say, this doubly-backward configuration is of interest since the three-wave symbiotic solitary waves can be generated from noise in the presence of a c.w. pump when the quadratic material is placed inside an optical parametric oscillator [14, 15, 16, 17, 18, 19]. With a c.w. pump the singly backward OPO yields stationarity for the backward wave. Nevertheless when the pump is a pulse, the demonstrated MOPO experimental configuration generates a coherent backward pulse in the absence of external feedback. Note that stationarity of the singly backward configuration in a c.w. pumped short length device is not contradictory with the theoretical existence of backward solitary solutions when the initial condition is localized [6]. Moreover, a coherent solitary structure can be sustained from a highly incoherent pump and a co-propagating wave [27]. This phenomenon relies on the advection between the interacting waves and leads to the formation of a novel type of three-wave parametric soliton composed of both coherent and incoherent fields. In section 5 we will consider this mechanism by proposing the generation of a coherent backward pulse from an incoherent pump pulse in two BMOPO configurations, among which the first one refers to the experimental configuration demonstrated in Refs. [24, 25, 26].

We thus show that the BMOPO system is characterized, as a general rule, by the generation of a highly coherent backward field, despite the high degree of incoherence of the pump field. In substance, the incoherence of the pump is shown to be transferred to the co-moving field, which thus allows the backward field to evolve towards a highly coherent state. The incoherent pump in the BMOPO dynamics is numerically simulated with a new numerical scheme that solves the coupled wave equations in the counterpropagating configuration in the presence of group-velocity dispersion (GVD) by combining the trajectories method for the nonlinear three-wave interaction and fast Fourier transformation (FFT) to account for the GVD effects. We propose realistic experimental conditions that may be implemented with currently available technology and in which backward coherent wave generation from incoherent excitation may be observed and studied.

We have already shown, by both analytical and numerical treatments of the degenerate backward OPO in the QPM decay interaction between a c.w. pump and a backward signal wave, that the inhomogeneous stationary solutions are always unstable, whatever the cavity length and pump power values are above threshold of a singly resonant OPO. Starting from any initial condition, the nonlinear dynamics exhibits self-pulsing of the backward signal with unlimited amplification and compression. Above a critical steepening of the backward pulse, dispersion may saturate this singular behavior leading to self-modulated solitary structures [17] [28].

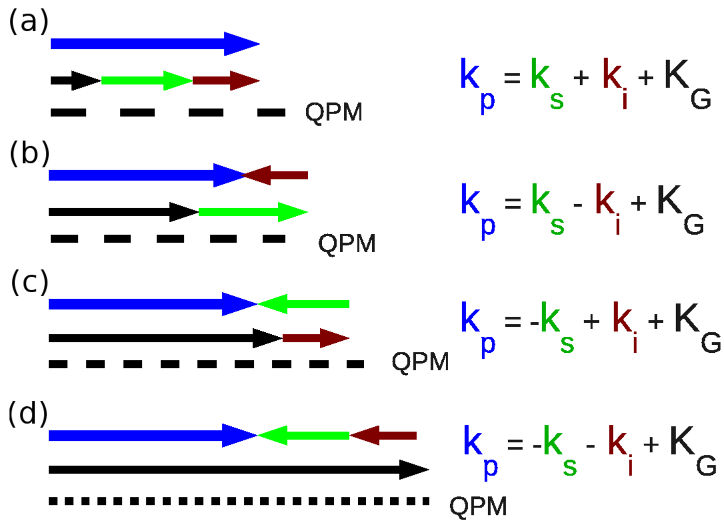

Fig. 1: Wave vector diagrams (momentum conservation) for the non-degenerate three-wave interaction in: (a) a three-wave forward configuration; (b) a singly backward idler configuration; (c) a singly backward signal configuration; and (d) a doubly backward (signal and idler) configuration. As we can see the QPM grating show a decreasing phase-reversal period for the nonlinear susceptibilty represented by the bold broken lines under each configuration.

In this paper we show, by a stability analysis of the non-degenerate backward OPO [18, 19], that the previous particular behavior of unconditional temporal instability of the degenerate backward OPO is removed for a finite temporal walk-off between the counter-propagating signal and idler waves, and that we now obtain a regular Hopf bifurcation like in the Brillouin fiber-ring laser [10]. We will consider self-structuration of three-wave solitary waves in such a backward OPO with absorption losses.

For a c.w. pumped OPO near degeneracy a unique control parameter L governs the dynamical behaviour; it is shown that at a critical interaction length L_{crit} the inhomogeneous stationary solution bifurcates towards a time-dependent oscillatory solution. This critical length is finite if and only if we take into account a finite group velocity delay between both backward propagating waves $\Delta v = |v_s - v_i| \neq 0$ (or temporal *walk-off*), where v_s and v_i are the signal and idler group velocities. Moreover, for longer interaction lengths the dynamics gives rise to the generation of the backward three-wave soliton, whose stability is also ensured by this finite temporal walk-off Δv, without requiring additional saturation mechanisms like the dispersion effect. This *scenario* is confirmed by numerical simulations of the nonlinear dynamic equations, and an excellent agreement is obtained (near the degenerate configuration) for the value of L_{crit} evaluated from the stability analysis and that one obtained from the dynamical simulation. The general fully non-degenerate configuration involves more complicated mathematics because a set of control parameters are required and we only show several dynamical behaviours resulting from the three-wave numerical model. We will conclude this review by considering some dynamical behaviours of the backward mirrorless OPO pumped with an incoherent pulse, because up to now this configuration is the only one in which backward MOPO experiments have been performed.

The paper is organized as follows. In section 2 we recall the three-wave model governing the spatio-temporal evolution of the slowly varying envelopes of the pump and the backward signal and idler waves. We also recall the analytical solutions in the form of propagating dissipative solitary waves propagating backward with respect the cw-pump under a QPM three-wave interaction. In section 3 is presented the stability analysis of the nonlinear inhomogeneous stationary solutions of the non-degenerate backward OPO for finite temporal walk-off. Numerical dynamics of the self-structuration of symbiotic three-wave solitons leading to stable self-pulsing regimes is shown in section 4. Finally, the numerical dynamics of the pulsed BMOPO under incoherent pump excitation is discussed in section 5.

2 Three-wave model and analytical solitary-wave solutions

The spatio-temporal evolution of the slowly varying envelopes of the three resonant counter-streaming interacting waves $A_j(x,t)$, for a non-degenerate OPO, is given by

$$\begin{aligned}(\partial_t + v_p\,\partial_x + \gamma_p + i\beta_p\partial_{tt})\,A_p &= -\,\sigma_p A_s A_i\\ (\partial_t - v_s\,\partial_x + \gamma_s + i\beta_s\partial_{tt})\,A_s &= \sigma_s A_p A_i^*\\ (\partial_t - v_i\,\partial_x + \gamma_i + i\beta_i\partial_{tt})\,A_i &= \sigma_i A_p A_s^*\end{aligned} \tag{1}$$

where $A_p(\omega_p,k_p)$ stands for the c.w. pump wave, $A_s(\omega_s,k_s)$ for the backward signal wave, and $A_i(\omega_i,k_i)$ for the backward idler wave. The resonant conditions in one-dimensional configuration realize the energy conservation,

$$\omega_p = \omega_s + \omega_i, \tag{2}$$

and the momentum conservation,

$$k_p = -k_s - k_i + K_G, \tag{3}$$

where $K_G = 2\pi/\Lambda_{QPM}$ and Λ_{QPM} is the grating pitch for the backward quasi-phase matching [cf. 1(d)]. The group velocities $v_j\ (j = p,s,i)$ as well as the attenuation coefficients γ_j and dispersion coefficients $\beta_j \equiv v_j\beta_{2,j}/2$ are in general different for each wave. Equations (1) also hold for standard forward phase-matching configurations in which case all the signs of the velocities $v_{s,i}$ are positive [cf. 1(a)]. For the singly backward idler (or backward signal) configuration the momentum conservation (3) must be replaced by (17). These configurations are shown in figure 1(b)(c). The nonlinear coupling coefficients are $\sigma_j = 2\pi d_{eff} v_j/(\lambda_j n_j)$, where n_j is the refractive index at frequency ω_j, wavelength λ_j and d_{eff} is the effective nonlinear susceptibility. The chromatic dispersion is also taken into account in equations (1); this is necessary when the generated temporal structures are sufficiently narrow. The effects of group velocity dispersion (GVD) are represented by the second derivatives with respect to time, so that the dispersion parameters are given by $\beta_j = |v_j|k_j''$ where $k_j'' = (\partial^2 k/\partial\omega^2)_j$, k being the wave vector modulus, $k = n(\omega)\omega/c$.

2.1 Solitary Wave Solution

In the absence of dispersion ($\beta_j = 0$) equations (1) have been extensively studied in the literature. Their solitary wave solutions have been first derived in the absence of dissipation ($\gamma_j = 0$) [2, 6, 3]. In the context of stimulated scattering in nonlinear optics, the existence of dissipative solitary waves when one of the velocities $v_{s,i}$ is zero (*e.g.* $v_i = 0$) has also been shown [9, 29]. More recently, Craik *et al.* have proved, for the particular case of degenerate three-wave interaction,

that solitary waves still exist in the presence of dissipation [30]. On the basis of these previous theoretical works, we have calculated from equations (1) a particular analytical solution of the dissipative symbiotic solitary waves of the non-degenerate parametric three-wave interaction. Looking for a solitary wave structure induced by energy transfer from the pump wave to the signal and idler pair, we have to assume zero loss for the pump ($\gamma_p = 0$). It is the only way to keep constant the energy transfer that compensates here for the signal and the idler losses, so as to generate stationary field structures. If γ_p was not zero, the pump wave would experience an exponential decay giving rise to a vanishing energy of the three-wave structure that prevents the formation of a stationary solitary wave state.
When $\gamma_p = 0$ it is easy to find by substitution the following solution to equations (1):

$$\begin{aligned} A_p &= \delta - \beta \tanh\left[\Gamma(x+Vt)\right] \\ A_s &= \eta\Gamma \operatorname{sech}\left[\Gamma(x+Vt)\right] \\ A_i &= \kappa\Gamma \operatorname{sech}\left[\Gamma(x+Vt)\right] \end{aligned} \tag{4}$$

where β is the only free parameter. All other parameters depend on the material properties and on β. One finds $\delta = [\gamma_s\gamma_i/\sigma_s\sigma_i]^{1/2}$, $\Gamma = \beta[\sigma_i\sigma_s/(V-v_s)(V-v_i)]^{1/2}$, $\eta = [(V+v_p)(V-v_i)/\sigma_i\sigma_p]^{1/2}$, $\kappa = [(V+v_p)(V-v_s)/\sigma_s\sigma_p]^{1/2}$, and $V = (v_s/\gamma_s - v_i/\gamma_i)/(1/\gamma_s - 1/\gamma_i)$. This last expression shows that the velocity V of the solitary wave is fixed by the material parameters, unlike in the nondissipative case where V is undetermined [2]. Let us point out that, in order to keep Γ real, the solitary wave must be either superluminous, $V > max(v_s, v_i)$, or subluminous, $V < min(v_s, v_i)$. Note that the superluminous velocity does not contradict by any means the special theory of relativity [9] even if the velocity V becomes infinite when the signal and idler waves undergo identical losses, $\gamma_s = \gamma_i$. This can be easily explained by remembering that the velocity of this type of symbiotic solitary wave is determined by the energy transfer rate, which depends on the shape of the envelope of each component. The infinite velocity is here simply due to the fact that the width of the solitary wave Γ^{-1} also becomes infinite for $\gamma_s = \gamma_i$. However, we shall see that this symmetrical solution is not the more general one and it is not an attractor solution for a large variety of parameter values. In section 4 we will present another self-similar structure for the near-degenerate backward interaction which does not present a divergence for $\gamma_s = \gamma_i$. The free wave parameter β fixes, in combination with the material parameters, the amplitude and the width of the solitary wave. According to the first equation of (4), β is determined by the initial pump amplitude $A_p = E_p(x = -\infty) = \beta + \delta$. In practice, this means that, for a given material, the solitary wave is completely determined by the pump intensity at the input face of the crystal. Note that if the losses are such that $\delta > \beta$ the solitary wave no longer exhibits a π-phase change [8], contrary to the nondissipative case [2].

Figure 2 shows a typical example of such a dissipative symbiotic solitary wave in a quasi-phase-matched backward three-wave interaction with $\lambda_p = 1$ μm, $\lambda_s = 1.5$ μm, $\lambda_i = 3$ μm, $\Lambda_{QPM} = 2\pi/K_G = 0.233$ μm, and with a pump field of amplitude $E_p = 0.25$ MV/m (*i.e.*, a pump intensity of $I_p = 10$ kW/cm^2) propagating in a quadratic $\chi^{(2)}$ material. It is obtained with the following typical values of the parameters : $d_{eff} = 20$ pm/V, $n_p = 2.162$, $n_s = 2.142$, $n_i = 2.098$, $v_p = 1.349 \times 10^8$ m/s, $v_s = 1.371 \times 10^8$ m/s, $v_i = 1.363 \times 10^8$ m/s, and the loss coefficients $\alpha_s = 2\gamma_s/v_s = 0.23$ m^{-1} and $\alpha_i = 2\gamma_i/v_i = 11.5$m^{-1}. Note that these parameters lead to a pulse width of approximately 10 picoseconds. Therefore, with such pulse durations one can expect that the zero pump loss approximation ($\gamma_p = 0$) is valid in practice in the neighborhood of the solitary wave structure. Indeed, if the characteristic absorption length v_p/γ_p is much larger than the pulse width Γ^{-1}, one can anticipate that the solitary wave undergoes adiabatic reshaping during propagation so as to adapt locally its profile to the exponentially decaying pump intensity.

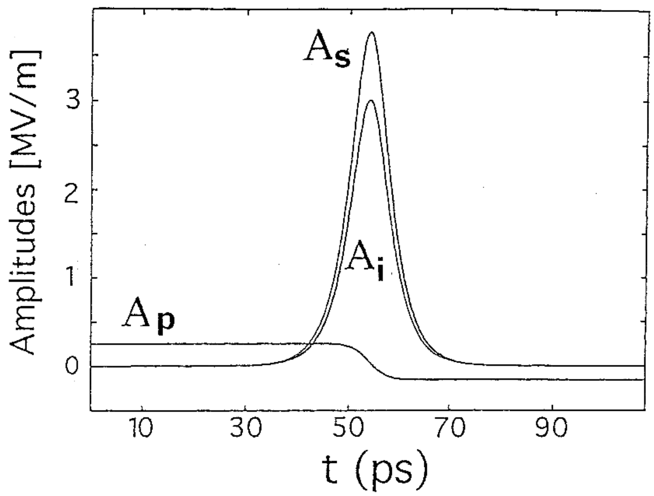

Fig. 2: Envelopes of the dissipative three-wave solitary solution.

3 Self-pulsing in a backward doubly resonant OPO

Let us point out that the self-structuration process requires backward interaction. The mechanism is similar to the Hopf bifurcation appearing in the counter-streaming Brillouin cavity [10]. Numerical simulations with the more usual forward phase-matching conditions only lead to the steady-state regime. This shows that the distributed feedback nature of the interaction plays a fundamental role in the pulse generation process. This observation is consistent with the conclusions of [23] where complex temporal pattern formation in backward-phase-matched second harmonic generation is studied and of our previous study of the degenerate backward OPO [28]. But in contrast to this last study, where no regular Hopf bifurcation was found by starting from the inhomogeneous stationary solutions, since above the threshold the perturbations always grow in time, we will show hereafter that in the non-degenerate backward OPO a regular Hopf bifurcation takes place. Below a critical parameter value, the inhomogeneous stationary solutions are stable, and above it the bifurcation leads to an also stable self-structured solitary wave. Our purpose in this section is to prove that in the non-degenerate configuration, the temporal walk-off, *i.e.* the group velocity delay between the signal and the idler waves, ensures a regular Hopf bifurcation and leads to a stable self-structuration of the three-wave envelopes.
For the sake of simplicity, we will focus here on the near-degenerate OPO regimes [18, 19]. However, our results are more general and can be extended to the fully non-degenerate case in a similar way. We present here several dynamical behaviours.

We start from the dimensionless form of equations (1) which describe the non-degenerate backward OPO in the quasi-phase-matching decay interaction between a pump and counter-propagating signal and idler waves. We write them near the degeneracy with temporal walk-off on only one field. This is not a restriction but it is more convenient for mathematical calculations. The general case can be recovered by an appropriate change of variables.
By introducing the following scalings:

$$u_p = \sqrt{1-d^2}\frac{A_p}{A_p^o},\ u_s = \sqrt{2(1-d)}\frac{A_s}{A_p^o},\ u_i = \sqrt{2(1+d)}\frac{A_i}{A_p^o},\ \ \tau = t/\tau_o,\ \ \xi = \frac{x}{\Lambda},\ \ L = \frac{\ell}{\Lambda} \qquad (5)$$

where A_p^o is the incident c.w. pump, $\tau_o = 2/(\sigma_p A_p^o)$ and $\Lambda = v_p\tau_o$ are the characteristic time and length and ℓ the cavity length, the dimensionless equations read:

$$\begin{aligned}
(\frac{\partial}{\partial\tau}+\frac{\partial}{\partial\xi}+\mu_p+i\tilde{\beta}_p\frac{\partial^2}{\partial\tau^2})u_p &= -u_s u_i \\
(\frac{\partial}{\partial\tau}-\frac{\partial}{\partial\xi}+\mu_s+i\tilde{\beta}_s\frac{\partial^2}{\partial\tau^2})u_s &= u_p u_i^* \\
(\frac{\partial}{\partial\tau}-\alpha\frac{\partial}{\partial\xi}+\mu_i+i\tilde{\beta}_i\frac{\partial^2}{\partial\tau^2})u_i &= u_p u_s^*
\end{aligned} \tag{6}$$

where $\alpha = v_i/v_p, \quad v_p = v_s, \quad \mu_j = \gamma_j\tau_o, \quad$ and $\quad \tilde{\beta}_j = \beta_j/\tau_o$. The full description of the OPO dynamics is obtained by taking into account, in addition to equations (6), the following boundary conditions for the doubly resonant cavity

$$u_s(\xi=L,\tau)=\rho_s\, u_s(\xi=0,\tau), \quad u_i(\xi=L,\tau)=\rho_i\, u_i(\xi=0,\tau), \quad u_p(\xi=0,\tau)=\sqrt{1-d^2} \tag{7}$$

where $\rho_s=\sqrt{R_s}$ and $\rho_i=\sqrt{R_i}$ are the amplitude feedback coefficients. Note that we have introduced the new coefficients $1\pm d$ by setting $d=(\sigma_s-\sigma_i)/\sigma_p$ and assuming a near-degenerate OPO configuration, *i.e.*, $\sigma_p \simeq \sigma_s+\sigma_i$.

3.1 Inhomogeneous stationary solutions

Without optical attenuation ($\mu_j=0$) and in the absence of dispersion ($\beta_j=0$), inhomogeneous stationary solutions $u_j^{st}(\xi),\ j=\{p,s,i\}$ can be obtained from equations (6) by setting $\partial/\partial\tau=0$. The assumption of zero loss parameters μ_j is not restrictive since the main dissipation in the OPO cavity comes from the finite feedback. In this case, the following conservation relations, also known as Manley-Rowe relations [31], hold

$$\begin{cases} |u_p^{st}|^2-|u_s^{st}|^2=\pm D_s^2 \\ |u_p^{st}|^2-\alpha|u_i^{st}|^2=\pm D_i^2 \end{cases} \tag{8}$$

For a doubly resonant OPO with the same feedback coefficient for the signal and idler fields, we have $D_s=D_i=D$. This leads to two types of stationary solutions : *(i)* $D^2=|u_p^{st}|^2-|u_s^{st}|^2=|u_p^{st}|^2-\alpha|u_i^{st}|^2$ and *(ii)* $D^2=|u_s^{st}|^2-|u_p^{st}|^2=\alpha|u_i^{st}|^2-|u_p^{st}|^2$.

In case *(i)*, the following inhomogeneous stationary solutions are obtained

$$\begin{aligned}
u_p^{st}(\xi) &= D\tanh^{-1}\left(\mathrm{arccotanh}(\frac{u_p^{st}(0)}{D})+\frac{D\xi}{\sqrt{\alpha}}\right) \\
u_s^{st\,2} &= \alpha u_i^{st\,2}=\frac{D^2}{\sinh^2\left(\mathrm{arccotanh}(\frac{u_p^{st}(0)}{D})+\frac{D\xi}{\sqrt{\alpha}}\right)}
\end{aligned} \tag{9}$$

while in case *(ii)*,

$$u_p^{st}(\xi)=D\frac{u_p^{st}(0)-D\tan(\frac{D\xi}{\sqrt{\alpha}})}{D+u_p^{st}(0)\tan(\frac{D\xi}{\sqrt{\alpha}})} \qquad u_s^{st}(\xi) = \sqrt{\alpha}u_i^{st}(\xi)=\frac{D\sqrt{1+\frac{u_p^{st\,2}(0)}{D^2}}}{\cos(\frac{D\xi}{\sqrt{\alpha}})+\frac{u_p^{st}(0)}{D}\sin(\frac{D\xi}{\sqrt{\alpha}})} \tag{10}$$

where $u_p^{st}(0) = \sqrt{1-d^2}$.
Let us consider the situation of short enough OPO cavities in order to avoid total depletion of the pump inside the cavity and to benefit from the monotonous gain of the singly pumped OPO; otherwise the signal and idler fields oscillate and may return part of this intensity to the pump. This is achieved by considering $D\xi \ll 1$. Thus, to the leading order, the inhomogeneous stationary solutions (10) are

$$u_p^{st}(\xi) \simeq \frac{u_p^{st}(0) - D^2\frac{\xi}{\sqrt{\alpha}}}{1 + u_p(0)\frac{\xi}{\sqrt{\alpha}}} \qquad \text{and} \qquad u_s^{st}(\xi) = \sqrt{\alpha}u_i^{st}(\xi) \simeq \frac{D\sqrt{1+\frac{u_p^{st\,2}(0)}{D^2}}}{1+\frac{u_p^{st}(0)\xi}{\sqrt{\alpha}}} \tag{11}$$

Manley-Rowe relations (8) are used at $\xi = 0$ and $\xi = L$, together with the boundary conditions to determine the integration constants. A second order algebraic equation for D^2 is obtained

$$aD^4 + bD^2 - c = 0 \tag{12}$$

with

$$a = L^2/\alpha,\ \ b = (1-R)(1+\sqrt{1-d^2}L/\sqrt{\alpha})^2 - 2\sqrt{1-d^2}L/\sqrt{\alpha},\ \ c = (1-d^2)[1-R(1+\sqrt{1-d^2}L/\sqrt{\alpha})^2]$$

Once D is determined from the above expression, $u_s(0)$ and $u_i(0)$ can be calculated via the Manley-Rowe relations (8).
Note that we will only consider the case *(ii)* configuration; case *(i)* can be analysed in a similar way.

3.2 Stability analysis of the inhomogeneous stationary solutions

Followinf Ref.[18] let us first perform the linear stability analysis of the inhomogeneous stationary solutions (10) with respect to space-time-dependent perturbations in the absence of dispersion and optical attenuation, through

$$u_j(\xi,\tau) = u_j^{st}(\xi) + \delta u_j(\xi)e^{-i\omega\tau} \quad \text{where} \quad j = p,s,i.$$

It is more convenient to introduce the new variables

$$P(\xi) = u_p^{st}(\xi), \quad S(\xi) = u_s^{st}(\xi), \quad I(\xi) = S(\xi)/\sqrt{\alpha} = u_i^{st}(\xi),$$
$$Z(\xi) = \delta u_p(\xi), \quad Y(\xi) = \delta u_s(\xi), \quad X(\xi) = \delta u_i(\xi),$$

where $P(\xi), S(\xi)$ and $I(\xi)$ stand for the inhomogeneous stationary solutions and $Z(\xi), Y(\xi)$ and $X(\xi)$ for the space-time-dependent perturbations. Thus, the linearized problem associated with equations (6) reads

$$\begin{aligned} \frac{\partial Z}{\partial \xi} - i\omega Z &= -S(X + \frac{Y}{\sqrt{\alpha}}) \\ \frac{\partial Y}{\partial \xi} + i\omega Y &= -PX - \frac{SZ}{\sqrt{\alpha}} \\ \alpha\frac{\partial X}{\partial \xi} + i\omega X &= -PY - SZ \end{aligned} \tag{13}$$

The stability analysis is performed by solving the perturbative equations (13) with the inhomogeneous stationary solutions and by taking into account the boundary conditions for the cavity. This gives rise to an eigenvalue problem with a dispersion relation for the complex frequency ω. Following [10], [28] and [18] we will look for the stability of the cavity modes with frequency $\Re(\omega) \simeq 2\pi N/L$ [N integer and L being the dimensionless length ℓ/Λ defined in (5)] yielding to mode instability whenever $\Im(\omega) > 0$.

3.2.1 Absence of walk-off

Let us first recall the situation in the absence of temporal walk-off; the signal and idler waves have the same group velocity leading to $\alpha = 1$ in equations (13). We proceed as in the degenerate case [28] and we obtain the following dispersion relation

$$a_o + b_o \sin(\omega L) + c_o \cos(\omega L) = 0 \qquad (14)$$

where the expressions of a_o, b_o and c_o are given in appendix A of Ref.[18]. It should be noted that equation (14) generalizes the dispersion relation in [28] for the degenerate case because it applies to the doubly-resonant backward OPO. The instability of each mode is determined from equation (14) when $\Im(\omega) > 0$. However, in the absence of walk-off, signal and idler perturbation equations are decoupled from the pump perturbation equation, and again it leads to unconditional temporal instability. We recall that this instability leads to the generation of a localized structure exhibiting unlimited amplification and compression [17] [28], whose collapse may be avoided by including the natural chromatic dispersion which is present in equations (1).

Since the required grating pitch for first order QPM is extremely small, we must increase the c.w. pump intensity when using higher order gratings in order to get an actual experimental configuration. Reference [21] gives a table with the threshold pump intensities and domain periods for the degenerate backward OPO in four periodic domain structures (KTP, $LiNbO_3$, GaAs/AlAs). Recently [32], it has been reported an experiment of first order QPM blue light generation at 412.66 nm, in a 20 mm long surface-poled Ti-indiffused channel waveguide in $LiNbO_3$ with c.w. pumping, using periodic domain structures as short as 1 μm. The authors have announced generation of 3.46 mW blue light for 70 mW of fundamental power. Based on such recent progresses in the poling technology of $LiNbO_3$ one can likely hope to experimentally realize the backward OPO with the allowed pump power for so short grating pitch. We will see in section 5 that a periodic domain of 800 nm has been obtained in a bulk PPKTP configuration to achieve for the first time the pulsed mirrorless OPO. For example, if $\Lambda_{QPM} = 0.5$ μm we may only use a c.w. pump power ten times higher (*i.e.* $I_{p,0} = 1$ MW/cm^2) for the same cavity length ℓ = 3.7 cm, same characteristic time $\tau_0 \simeq 0.28$ ns, and same low finesse $\rho_s = \sqrt{R} = 0.46$ as that given in the previous example. If we consider a pulse pump of FWHM of $\Delta t = 28$ ns instead of a c.w. beam we can even reach $I_{p,0}$ = 100 MW/cm^2 without optical damage [33] (yielding $\tau_0 = 28$ ps and $\Lambda = 0.37$ cm).

3.2.2 Finite temporal walk-off

When taking into account a finite temporal walk-off $\alpha \neq 1$, equations (13) are more complicated as the dynamics of the pump wave and the signal-idler pair is no longer decoupled. For the sake of simplicity let us consider $D = 0$, so that $P = S = \sqrt{\alpha} I = 1/(1/\sqrt{1-d^2} + \xi/\sqrt{\alpha})$. Note that $D = 0$ requires that $c = 0$ in equation (12). Since $d \ll 1$, it is the second factor in the same expression of c which vanishes leading to the relation $R = 1/(1+\sqrt{(1-d^2}L/\sqrt{\alpha})^2$. The first-order perturbed system becomes

$$\frac{d}{d\xi}\begin{pmatrix} Z \\ Y \\ X \end{pmatrix} = \begin{pmatrix} i\omega & -I & -S \\ -I & -i\omega & -P \\ -S/\alpha & -P/\alpha & -i\omega/\alpha \end{pmatrix}\begin{pmatrix} Z \\ Y \\ X \end{pmatrix}$$

This system of equations is numerically solved. Since the group velocity delay (temporal walk-off) of the signal and idler pair is small, we set $\alpha = v_i/v_p \simeq 1+\varepsilon$. We expand the solutions

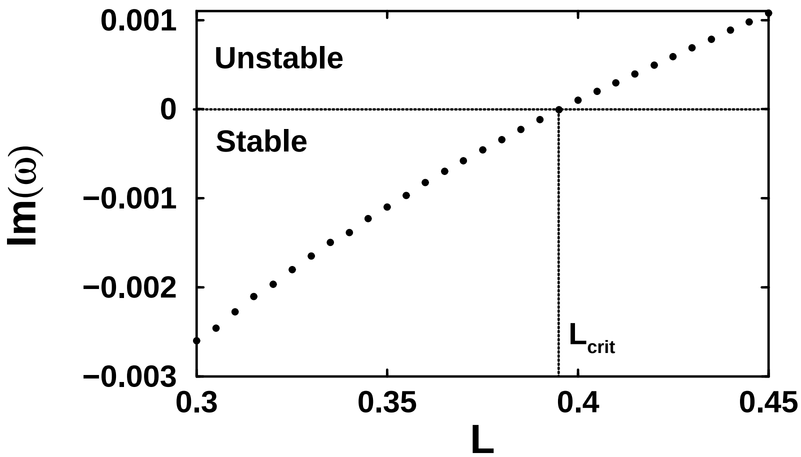

Fig. 3: Evolution of the imaginary part of the pulsation ω as a function of the length L close to the first cavity mode (with $\mathrm{Re}(\omega) \simeq 2\pi/L$). The transition from stable to unstable states is obtained for $L_{crit} \simeq 0.39$.

up to the second order in the small parameter ε. The second order is necessary to match the critical parameter value obtained at the Hopf bifurcation point by the numerical integration of the normalized governing equations (6); the first order in ε being insufficient to characterize the bifurcation point.
Through the boundary conditions, we obtain the dispersion relation:

$$\begin{aligned}\omega^3 y_o^2 y_L \quad &+ \Big[-\omega^3 y_o^2 y_L - i\omega^2 y_o L + \omega L\Big]\cos(\omega L) + \Big[i\omega^3 y_o^2 y_L + i\omega y_o - \omega^2 y_o L - 1\Big]\sin(\omega L) \\ - \quad & \frac{i\varepsilon}{8y_L(y_o\rho_o - y_L e^{-i\omega L})}\Big\{A_o e^{-2i\omega L} + B_o e^{-i\omega L} + C_o e^{i\omega L} + D_o\Big\} \\ - \quad & \frac{i\varepsilon^2}{24 y_L^2(y_o\rho_o - y_L e^{-i\omega L})}\Big\{A_1 e^{-2i\omega L} + B_1 e^{-i\omega L} + C_1 e^{i\omega L} + D_1\Big\} = 0 \end{aligned} \tag{15}$$

with $y_o = 1/\sqrt{1-d^2}$, $y_L = y_o + L$, $\rho_o = y_o/y_L$ is the amplitude feedback coefficient and L stands for the dimensionless length ℓ/Λ. The expressions of the different coefficients A_o, A_1, B_o, B_1, C_o, and C_1, which are functions of $\omega = \omega_r + i\omega_i$, y_L, and y_o are given in appendix B of Ref.[18]. First we recover, as it should be, the dispersion relation (14) when $\varepsilon = 0$ and $D = 0$. However, the non-degenerate backward OPO dispersion relation (15) shows that, in contrast to the degenerate case, there exist a stability domain of the inhomogeneous stationary solutions above threshold. Moreover, these solutions undergo a Hopf bifurcation, even near the degenerate configuration, for a critical lenght of the cavity. Figure 3 shows a typical example of a regular Hopf bifurcation with the parameters set to $d = 0.05$ and $\varepsilon = 1/128$. We have plotted $\Im(\omega)$ from equation (15) against the propagation length L near the first cavity mode ($\Re(\omega) \simeq 2\pi/L$). As can be seen from the figure, Hopf bifurcation occurs at $L_{crit} \simeq 0.39$. For $L \leq L_{crit}$ the inhomogeneous stationary solutions are stable (see figure 4) whereas if $L > L_{crit}$ the perturbations are amplified generating a new oscillatory localized structure (see figures 5 and 6).

4 Nonlinear dynamics of the doubly resonant backward OPO

In the previous section we have carried out the stability analysis of the inhomogeneous stationary solutions of the doubly resonant backward OPO near the degenerate configuration. This behavior may be generalized to the fully non-degenerate backward OPO provided that a finite temporal

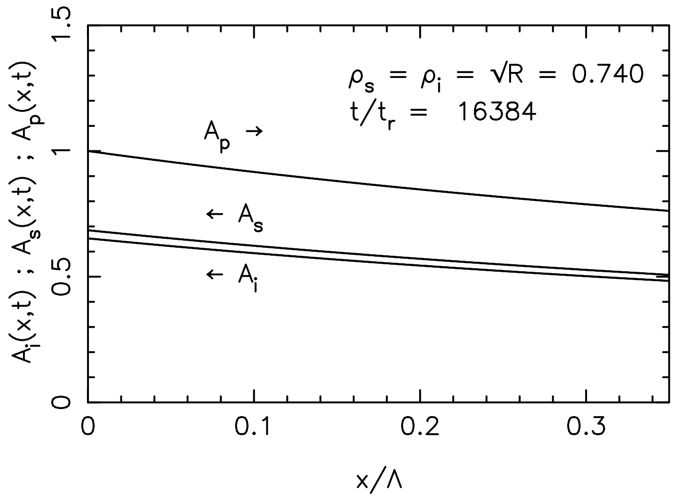

Fig. 4: Doubly resonant backward OPO: asymtotic stationary spatial profiles at round trip 16384 for $L = 0.35$ below critical length.

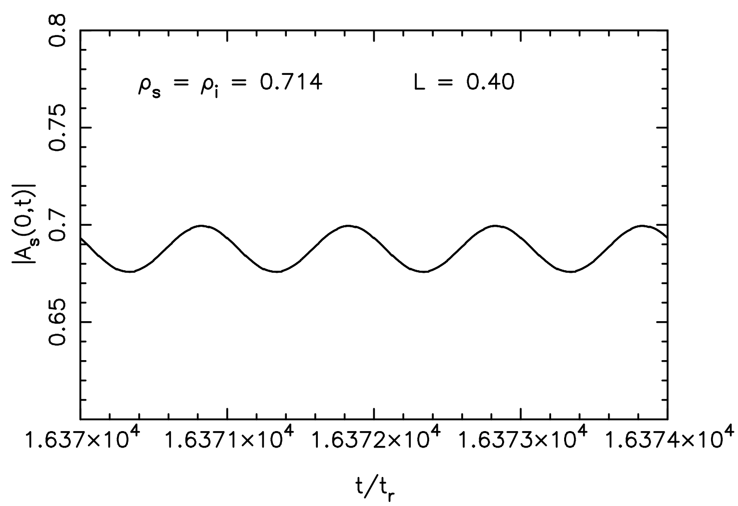

Fig. 5: Doubly resonant backward OPO: temporal oscillatory regime for $L = 0.4$ above critical length.

walk-off between the counter-propagating signal and idler waves is present . In this section we proceed as follows:
(i) we numerically check the previous analytical result in the near-degenerate OPO regime for $D = 0$;
(ii) we show that a dynamically critical bifurcation for $D \neq 0$ can be obtained with the same feedback parameter values ($\rho_s = \rho_i$) for both signal and idler waves;
(iii) we numerically investigate the self-pulsing regime for the doubly resonant backward OPO with different feedback parameter values ($\rho_s \neq \rho_i$) including perturbative dispersion.

To this end we have numerically integrated equations (6) with the boundary conditions (7). In order to better compare the dynamical behavior with the analytical one, we first neglect dispersion ($\tilde{\beta}_j = 0,\ j = p,s,i$) which is only a perturbative effect in the non-degenerate case, but we include a small dissipation ($\mu_j = 10^{-2}$). In order to dynamically investigate the near-degenerate OPO regime for $D = 0$, we start from the approximate stationary solutions (11) with a

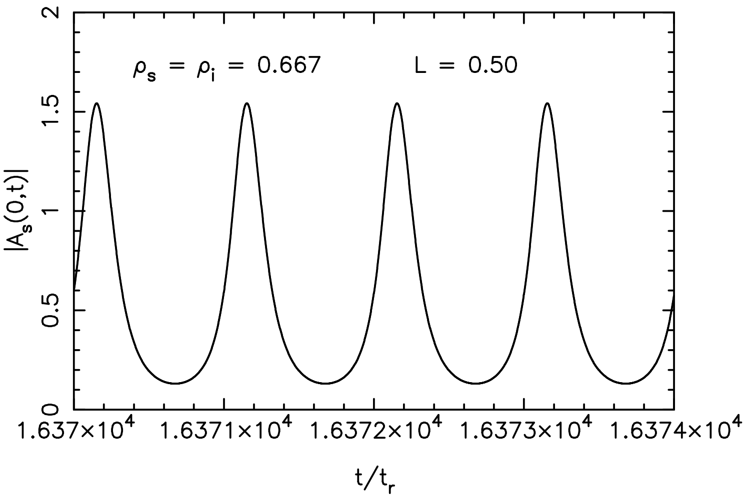

Fig. 6: Doubly resonant backward OPO: temporal pulsed regime for a length $L = 0.5$.

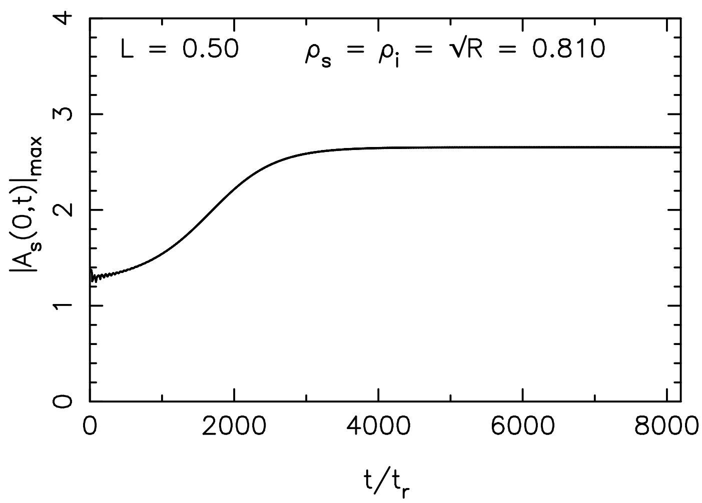

Fig. 7: Doubly resonant backward OPO: pulse maximum amplitude *vs.* number of round trips t/t_r (where $t_r = \ell/v_s$ is the round-trip time) at the output of the backward OPO cavity exhibiting stable saturation at a constant amplitude.

group velocity difference (temporal walk-off) $|v_s - v_i|/v_p = 1/128$. In the near-degenerate OPO case, the feedback $R = |\rho_s|^2 = |\rho_i|^2$ is related to the dimensionless length L through the relation $u_p^2(L) - Ru_s^2(L) = D^2$, which is now simply reduced to $R = [1 + L\sqrt{(1-d^2)/\alpha}]^{-2}$. Therefore, we may investigate the near-degenerate OPO dynamics by varying the control parameter L from 0.25 to 0.5. As expected from the stability analysis, we now find a regular Hopf bifurcation of the stationary state towards a time-dependent oscillatory state for a critical length L_{crit} between 0.35 and 0.4, in contrast to the full degenerate case [28] or to the near-degenerate case $D = 0$ in the absence of temporal walk-off [*cf.* section 3.2.1], where no Hopf bifurcation exists. The stationary spatial profiles are shown in figure 4 after 16384 round trips for $L = 0.35$. This stationary state bifurcates towards a stable oscillatory regime as illustrated in Fig. 5 for $L = 0.4$. For a larger length L (and correspondingly smaller feedback R) we obtain pulsed regimes as that shown in figure 6 whose stability is ensured by the finite temporal walk-off too, without taking into account any dispersion effect (*cf.* Fig.7).

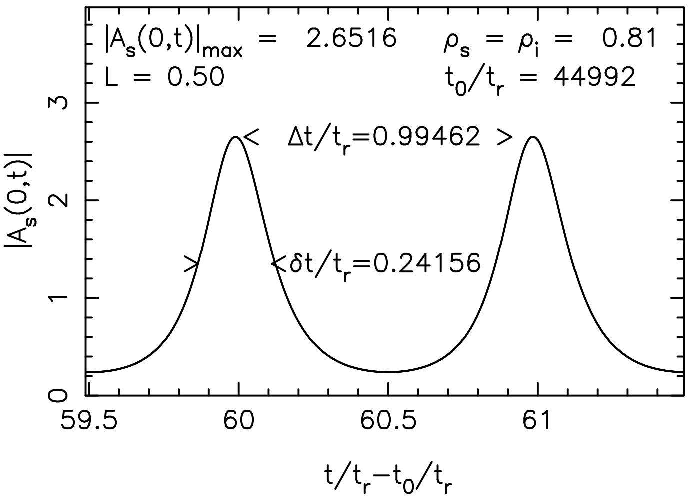

Fig. 8: Doubly resonant backward OPO: temporal evolution of a pulse train at the output of the OPO cavity. Pair of two consecutive pulses at round trip $t/t_r = 28608$ for $L = 0.5$ and $\rho_s = \rho_i = 0.81$. The amplitude is measured in $|A_{p,o}|/\sqrt{2}$ units.

The dynamical equations (6) allow us to look further for $D \neq 0$, while the control parameter L (since R is only a function of K for $D = 0$) splits now into two control parameters L and R related through $u_p^2(L) - Ru_s^2(L) = D^2$. For $L = 0.25$ we obtain the Hopf bifurcation between $\sqrt{R} = 0.80$ and 0.81, while for $L = 0.5$ it happens between $\sqrt{R} = 0.81$ and 0.82, the pulsed regimes corresponding to lower feedback favors the localization of the structure [11]. For a typical pulsed regime at $L = 0.5$ and $\sqrt{R} = 0.81$, we show in figure 7 the saturation of the pulse maximum amplitude with time when starting from the stationary state, and in figure 8 a pair of two consecutive pulses in the asymptotic stable state (the width δt is measured in $t_r = \ell/v_s$ units). As can be seen from figure 9 the solitary structure is now composed of two embedded pulses of nearly identical amplitudes moving together, the constant spatial shift between them corresponds to the temporal walk-off (or different group velocities). The trapping between the signal and idler envelopes yields the new self-similar structure moving at a characteristic velocity, which is composed of the couple of embedded pulses maintaining constant spatial shift between them in spite of the different velocities of both waves.

Let us consider a physical application. In comparison to the type I (e-e) polarization interaction in $LiNbO_3$ proposed in [28] for the full-degenerate case, we may now consider a type II (e-o-e) polarization interaction in order to move away from the degeneracy and to obtain a finite group velocity delay (or temporal walk-off) between the signal and the idler waves. For the same quadratic $\chi^{(2)}$ material, same pump wave (e-polarized) at $\lambda_p = 0.775\ \mu$m, the same idler wave (e-polarized) at $\lambda_i = 1.55\ \mu$m, but now a signal wave (o-polarized) at $\lambda_s = 1.55\ \mu$m having a different refractive index, the group velocity dispersion ensures a finite temporal walk-off between both backward waves. For a first order QPM in $LiNbO_3$ the grating pitch is as small as $\Lambda_{QPM} = 2\pi/K_G = 0.177\ \mu$m. For a c.w. pump field $E_p = 0.725$ MV/m (*i.e.*, a pump intensity of $I_p = 100$ kW/cm^2) propagating in this configuration we have the following values of the parameters [33]: $d_{eff} = 6$ pm/V, $n_p = 2.181$, $n_s = 2.212$, $n_i = 2.140$, $v_p = 1.317 \times 10^8$ m/s, $v_s = 1.323 \times 10^8$ m/s, $v_i = 1.372 \times 10^8$ m/s, $\gamma_p = 4.6 \times 10^8$ s^{-1}, and $\gamma_s = \gamma_i = 3.1 \times 10^8$ s^{-1}. The nonlinear characteristic time yields $\tau_0 = (\sigma_p A_p/2)^{-1} \simeq 0.94$ ns, and the nonlinear characteristic length $\Lambda = v_p \tau_0 = 12$ cm. We have taken cavity lengths running from 3 cm ($L = 0.25$) to 6 cm ($L = 0.5$) and we obtain a temporal width of the solitary pulses of the order of 100 ps.

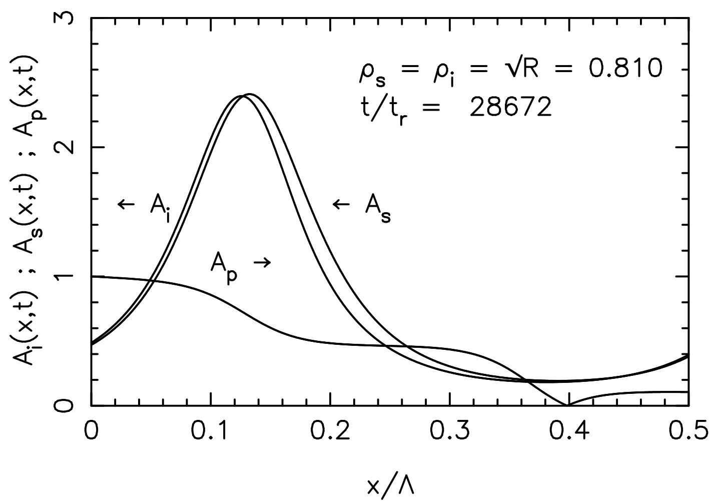

Fig. 9: Doubly resonant backward OPO: spatial profiles for the three wave amplitudes at round trip 28672.

Critical bifurcation parameters for doubly resonant backward OPOs with different nonlinear coupling coefficients σ_j and different feedback parameter values ($\rho_s \neq \rho_i$) may be obtained through the general dynamical equations (1) with boundary conditions (7). Figure 10 displays a typical self-pulsing regime for $\sigma_s/\sigma_p = 0.675$, $\sigma_i/\sigma_p = 0.350$, $L = 1$, $\tilde{\beta}_j = 10^{-6}$, $j = \{p, s, i\}$, $\rho_s = 0.9$ and $\rho_i = 0.6$. As can be seen from this figure the predicted stability of the self-pulsing regime is not affected by the presence of chromatic dispersion.

5 Backward coherent pulse from incoherently pumped mirrorless OPO

The numerical dynamics of a c.w. pumped singly backward OPO, experimentally adapted for an integrated cavity or IOPO (see for exemple [34, 35, 36, 37]), either for counter-propagating signal or for counter-propagating idler does not generate backward solitary structures. Even for high OPO finesses the laser output is always stationary. Note that this does not contradict the existence of backward solitons in singly counter-propagating configurations if the backward wave is initially localized [2] [3] [27]. It simply means that such solitary waves cannot be spontaneously generated from quantum noise and a c.w. pump. Nevertheless, we shall see in this section that the singly backward OPO configuration is interesting from another point of view, namely the generation of a coherent backward pulse from an incoherent pump pulse. In this section we will show that recent experimental demonstration of a backward mirrorless optical parametric oscillator (BMOPO) with a pump pulse in the quasi-phase-matched (QPM) periodic polarized $KTiOPO_4$ crystal [24, 25, 26] opens the way for achieving ultra-coherent output from a highly incoherent pump pulse. In a first time we consider a coherently phase modulated pump because in the experiments the broadening of the pump is done via a coherent chirp [25, 26].
The pump phase modulations are transferred to the co-propagating wave moving at nearby the same group velocity of the pump through the *convection-induced phase-locking mechanism* [27] [39] [40] [42]. For the highly incoherent pump we present the case of perfect group-velocity matching of the pump and the co-propagating idler wave, which may be achieved in a type I OPO for a pump at 1.060 μm, a counterpropagating signal at 1.676 μm and an idler at 2.882 μm. We will show that the degree of coherence of the backward signal field turns to be more than three orders of magnitude greater than that of the incoherent pump, with approximately the same pump power and crystal length as in the experiments.

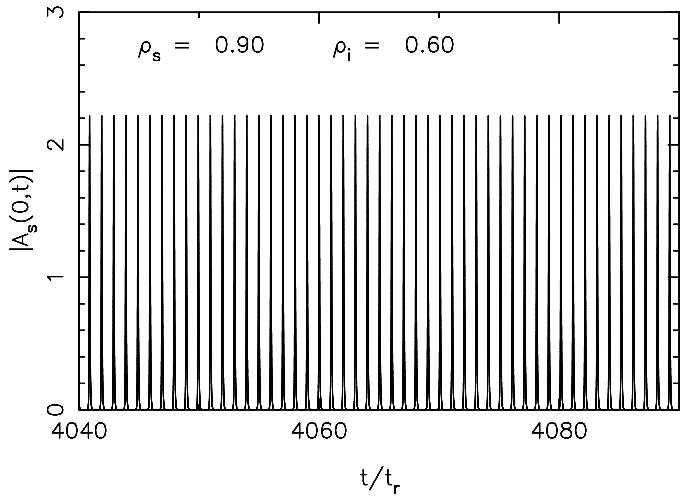

Fig. 10: Doubly resonant backward OPO: temporal amplitude signal output of the backward OPO in the stable asymptotic pulsed regime measured in cavity round trips t/t_r for $L = 1$, $\rho_s = 0.90$ $\rho_i = 0.60$ and $\tilde{\beta}_j = 10^{-6},\ j = p, s, i$.

Parametric interaction of counterpropagating optical waves has the unique property of automatically establishing distributed feedback without external cavity mirrors; the mirrorless optical parametric oscillator has been the object of several studies [31] [43] [21] [44]. The recent BMOPO experiments exhibit useful spectral properties and have been performed in a configuration of type I at $\lambda_p = 0.8616$ μm, $\lambda_s = 1.2179$ μm and $\lambda_i = 2.9457$ μm with a grating period of $\Lambda_{QPM} = 0.8$ μm. This singly backward configuration overcomes the extremely low sub-μm grating periodicity required for the doubly backward OPO (*cf.* sections 3 and 4).

We have already proposed two experimental configurations in type II singly resonant KTP IOPO's [40] and in a type I $\{eee\}$ singly resonant Ti:LiNbO$_3$ IOPO [42], to show the locking mechanism in standard high finesse forward propagating OPO's feeded with a c.w. pump. We will also show in this section the feasibility of coherent backward generation from an incoherent pump pulse in a mirrorless BMOPO configuration feeded with a pulse pump.

5.1 MOPO threshold and dynamical equations

A theoretical model yields an estimate of the MOPO threshold for counterpropagating plane waves [21], which is reached when the spatial gain exceeds $\pi/2$:

$$I_{pth} = \frac{\varepsilon_0 c n_p n_s n_i \lambda_s \lambda_i}{2\ell^2 d_{eff}^2} \tag{16}$$

where ε_0 is the permittivity of free space, ℓ the interaction length, d_{eff} the effective quadratic nonlinear coefficient, and $n_{s,i}$, $\lambda_{s,i}$ the respective signal and idler refractive index and wavelength. For example, for a PPKTP crystal of $d_{eff} = 8$ pm/V we have:

$$\ell = 1 \text{ cm} \quad \Longrightarrow \quad I_{pth} = 0.64 \text{ GW/cm}^2$$

$$\ell = 6.5 \text{ mm} \quad \Longrightarrow \quad I_{pth} = 1.08 \text{ GW/cm}^2$$

The momentum mismatch for the optical parametric generation process for the singly backward QPM configuration yields now

$$k_p = \pm k_s \mp k_i + K_G, \tag{17}$$

where $(+k_s, -k_i)$ stands for backward idler propagation and $(-k_s, +k_i)$ for backward signal propagation [*cf.* figure 1 respectively (b) and (c)], whith a resulting larger QPM grating period as that of the doubly backward OPO configuration. The schematic vector diagram and periodically domain-inverted ferroelectric crystal of the counterpropagating interaction are shown in figure 1, and equations (1) become:

$$\begin{aligned} (\partial_t + v_p\ \partial_x + \gamma_p + i\beta_p\partial_{tt})\, A_p &= -\ \sigma_p A_s A_i \\ (\partial_t \pm v_s\ \partial_x + \gamma_s + i\beta_s\partial_{tt})\, A_s &= \ \ \sigma_s A_p A_i^* \\ (\partial_t \mp v_i\ \partial_x + \gamma_i + i\beta_i\partial_{tt})\, A_i &= \ \ \sigma_i A_p A_s^*. \end{aligned} \tag{18}$$

with respectively $(+v_s, -v_i)$ for the backward idler propagation and $(-v_s, +v_i)$ for the backward signal propagation.

The input parameters in the model are the properties of the nonlinear medium and the pump amplitude at the input face, $\mathbf{A_p}(x=0,t)$, generating outputs of $\mathbf{A_p}(x=L,t)$, and either for the backward idler configuration [Fig.1(b)] $\mathbf{A_s}(x=L,t)$ and $\mathbf{A_i}(x=0,t)$ or for the backward signal configuration [Fig.1(c)] $\mathbf{A_s}(x=0,t)$ and $\mathbf{A_i}(x=L,t)$, where $x=0$ and $x=L$ denote the positions of the input and output faces with respect to the pump beam. For the numerical treatment of the coupled wave equations for counter-propagating interactions, the standard split-step one-directional integration algorithm, usually employed for co-propagating interactions, is not suitable due to the fact that Eqs.(19) represent a problem with two simultaneous, but spatially separate, boundary conditions, i.e., the pump wave and the copropagating wave (either the signal or the idler) are initially given at one end of the medium, while the backward wave (either the idler or the signal) is input from the other end of the medium. For such problems, there are two main appropriate numerical methods: the shooting or trajectories method and the relaxation method. For the problem at hand, the trajectories method is more convenient, whereby we eventually want to simulate a counterpropagating three-wave mixing process driven by a pump field with a quasi-random phase distribution. The trajectories method with the use of a Runge-Kutta algorithm has been extensively used for the treatment of stimulated Brillouin back-scattering problems [7, 8]. The linewidth narrowing experimentally studied in Brillouin lasers [45] has been simulated in a Brillouin fiber-ring laser with the help of this method [9]. In that case, it is the acoustic wave that absorbs the phase fluctuations of the pump and allows the backward Stokes wave to increase its coherence. In order to numerically integrate the nonlinear counterpropagation dynamics in a MOPO in the presence of group-velocity dispersion (GVD), which introduces second-order time derivatives, we have developed a new numerical scheme which combines the trajectories method with fast Fourier transformation (FFT) to account for the GVD effects in the spectral domain [47].

The scheme accurately conserves the number of photons and the Manley-Rowe invariants of Eqs.(19). As in the standard split-step approach, the evolution of Eqs.(19) is for each time step (typically 1 fs long) first treated by linear propagation of the fields in the Fourier domain, thereby accounting for the GVD effects and the group-velocity difference between the pump and the co-propagating wave. The originality with respect to the standard split-step schemes with multiply-repeated FFT and inverse FFT procedures where exponential spectral cut-off filtering

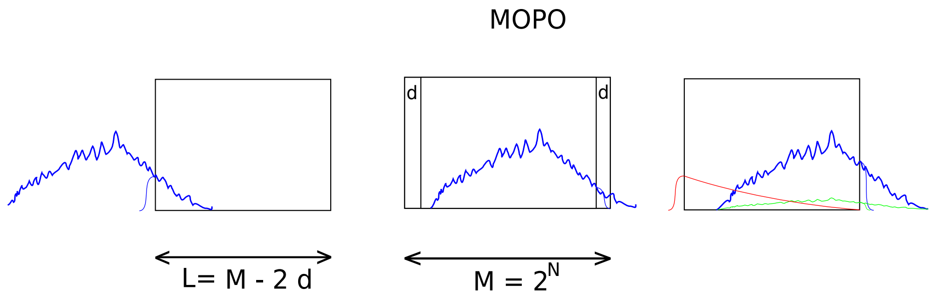

Fig. 11: Scheme for the Runge-Kutta-FFT numerical model for the backward mirrorless OPO.

is introduced at the edges of the spectrum, is that we here introduce smoothed exponentially-decreasing prolongations of the outgoing complex amplitudes (over a length d) in the x-space of the MOPO crystal of length L in order to render a periodic problem (cf. Fig. 11). Thus the FFT is correctly performed in the extended interaction domain of length M = L + 2d without arbitrary cut-offs. Then, after inverse FFT, the backward nonlinear interaction with spatially separate boundary conditions is treated by using the trajectories method. Integration over the trajectories in the nonlinear step of the algorithm was performed by using a 4th -order fixed-step Runge-Kutta method. The space- time is discretized in 2N points with N = 16 to 18, which, for instance, when N = 16 allows for a total bandwidth of 35 THz with the resolution of 0.5 GHz. The algorithm is seeded by an appropriate model pump field entering from one side of the nonlinear crystal and homogeneously spatially-distributed signal and idler fields with powers corresponding to a half photon per mode and with random phases, representing quantum noise. During the field evolution, we checked that the Manley-Rowe invariants were preserved to the accuracy of better than 10^{-5}, even after numerically evolving Eqs.(19) over 6×10^{6} time steps. The results obtained with our method were compared with those obtained using a 4th -order finite-difference scheme. For the chirped input pump pulse, where differentiability is ensured, the same quantitative results are obtained with both methods. The latter scheme, however, is not adapted for incoherent pulses.

5.2 BMOPO I actual experimental realization

The QPM three-wave resonant coupling in the experimental achieved backward MOPO of type I in a bulk PPKTP crystal [24, 25, 26] correspond to the following parameters [46]:

$$\lambda_p = 0.8616\mu\text{m};\ n_p = 1.8400;\ v_p/c = 0.5269;\ \beta_{2,p} = 0.2473\ \text{ps}^2/\text{m}$$

$$\lambda_s = 1.2179\mu\text{m};\ n_s = 1.8243;\ v_s/c = 0.5372;\ \beta_{2,s} = 0.1343\ \text{ps}^2/\text{m}$$

$$\lambda_i = 2.9457\mu\text{m};\ n_i = 1.7806;\ v_i/c = 0.5334;\ \beta_{2,i} = -0.6413\ \text{ps}^2/\text{m}$$

where

$$\Lambda_{QPM} = [\frac{n_p}{\lambda_p} - \frac{n_s}{\lambda_s} + \frac{n_i}{\lambda_i}]^{-1} = 0.8012\ \mu\text{m}$$

$$\Delta v/v_s = |v_p - v_s|/v_s = 0.0195,$$

and the counter-propagation interaction corresponds to figure 1(b).

Let us show the dynamical behaviours for a BMOPO of 6.5 mm length pumped with a 54 ps pulse duration of I_p = 2.34 GW/cm^2 maximum intensity. BMOPO operation in a PPKTP crystal of period $\Lambda = 800$ nm is simulated with a linearly-chirped pump pulse with a central wavelength of 861.7 nm. The input pump amplitude is chosen to be Gaussian and given by

$$\mathbf{A_p}(x=0,t) = \mathbf{A_p^0}\exp[i\phi_p(t)]\exp\{-2\ln 2[(t-t_0)/\Delta t_0]^2 \tag{19}$$

The spectral and temporal shapes of the pulse are determined by the phase modulation, $\phi_p(t)$ and the FWHM temporal length, Δt_0. With a linear chirp, the phase modulation is quadratic in time, $\phi_p(t) = \alpha_2 t^2$, where the value of the chirp parameter $\alpha_2 = -0.244$ rad/ps^2 is chosen to obtain the chirp rate of $d\omega_p/dt = -0.49$ rad/ps^2. With this chirp, a temporal intensity FWHM of $\Delta t_0 = 52$ ps gives a FWHM spectral width of 4.04 THz.

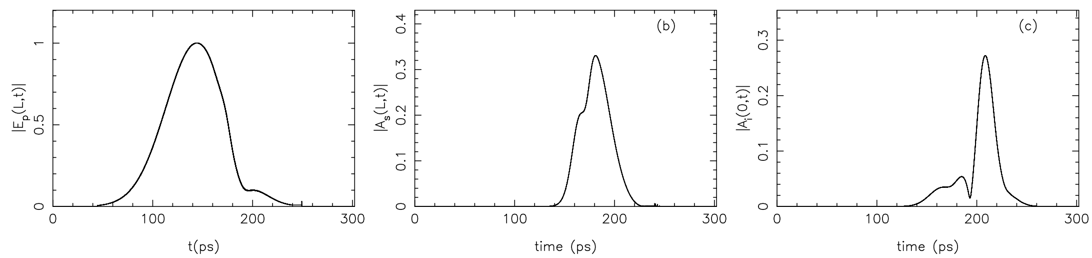

Fig. 12: BMOPO I: Temporal field amplitude output of pump (a), signal (b) and counterpropagating idler (c) waves in the achieved experimental configuration [26], for a pump of 52 ps temporal duration and 4.04 THz chirped pump bandwidth.

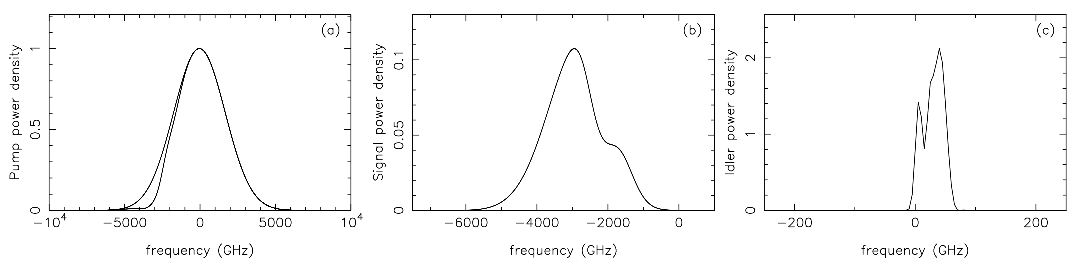

Fig. 13: (a) Undepleted input and depleted output pump spectrum of $\Delta\nu_p = 4.04$ THz, (b) the forward signal spectrum with $\Delta\nu_f = 1.78$ THz and (c) the backward idler spectrum with $\Delta\nu_b = 51$ GHz.

As the pump pulse enters the crystal, a forward signal and a backward idler are generated with similar spectral characteristics as those obtained in the experiment [26]. The temporal pump output amplitude and output co-propagating signal and backward idler amplitudes are illustrated in Fig 12. The pump and the parametric spectra at the pump intensity of 2.34 GW/cm^2 are illustrated in Fig 13, showing a backward idler with a spectral width of $\Delta\nu_i = 51$ GHz, which is narrow compared to the widths of the pump, $\Delta\nu_p = 4.04$ THz, and the forward signal, $\Delta\nu_s = 1.78$ THz. By integrating the spectra, it is found that the conversion into parametric waves here is $I_s(L)/I_p(0) = 0.036$ for the signal and $I_i(0)/I_p(0) = 0.014$ for the idler. As expected from the convection-induced phase-locking mechanism, the phase modulation in the pump is essentially transferred to the forward signal, while the phase of the backward idler is approximately constant.

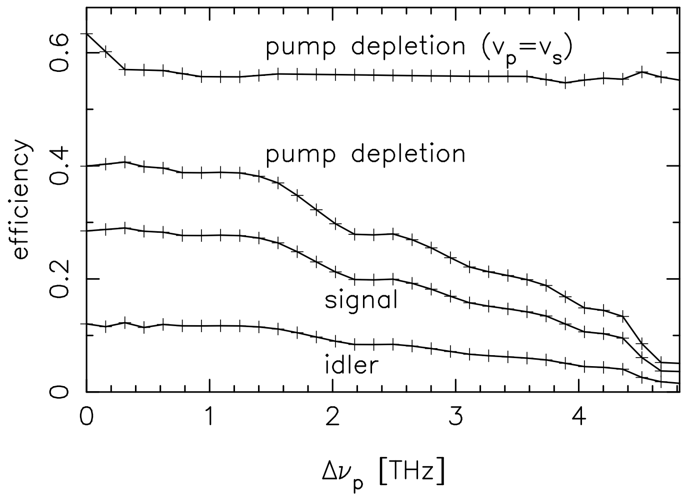

Fig. 14: Pump depletion, $1-I_p(L)/I_p(0)$, and conversion efficiencies for the signal, $I_s(L)/I_p(0)$, and for the idler, $I_i(0)/I_p(0)$, in the MOPO as function of the pump bandwidth for linearly-chirped pulses at the pump intensity of $I_p = 2.57$ GW/cm^2. The three lower curves correspond to the experimental condition, $|v_s - v_p|/v_s = 0.0195$, which clearly show a decrease in the efficiency as the pump bandwidth increases. The upper curve shows that the pump depletion is essentially independent of the pump bandwidth when $v_s - v_p = 0$.

By running simulations with pump pulses of different spectral widths, it is observed that the conversion efficiency decreases as the pump spectrum broadens when the group-velocity difference between the forward wave and the pump is the same as in the experiments. This behavior is due to the nonzero convective velocity $|v_p - v_s|$ of the co-moving waves, i.e. a finite temporal walk-off, which makes the spectral components in the signal move past those in the pump. On the other hand, for perfect group-velocity matching ($v_s = v_p = 0$), there is no temporal walk-off and the conversion efficiency is constant as the pump spectrum broadens, since the pump and the signal move at the same velocity. The pump depletion, $1-I_p(L)/I_p(0)$, and the conversion efficiencies into signal, $I_s(L)/I_p(0)$, and idler, $I_i(0)/I_p(0)$, were systematically investigated for linearly-chirped Gaussian pump pulses where the temporal pulse shape was held constant with a FWHM length of 52 ps and a peak intensity of 2.57 GW/cm^2. The spectral width was controlled by varying the chirp parameter α_2 from 0 to -0.30 rad/ps^2, corresponding to a FWHM bandwidth from the transform limit up to about 5 THz. In Fig. 14, the three lower curves show how the pump depletion and the conversion efficiency into signal and idler decrease as the pump bandwidth increases. Each point on the curves corresponds to a mean value over a set of simulations with random initial phases, i.e. the phase modulation is given by $\phi(t) = \alpha_2 t^2 + \phi_0$, where ϕ_0 is a random number. The efficiency is slightly different for each choice of ϕ_0 and the value typically varies within the vertical bar of the plus signs associated to each point. At some points, there is an apparent increase in the efficiency with an increased pump bandwidth, which is due to the limited set of random initial phases $(n = 6)$ used for the averaging. However, the main behavior is that a broader pump input spectrum decreases the efficiency of the BMOPO process when the group-velocities of the forward wave and the pump are not matched. The upper curve in Fig. 14 shows the pump depletion when the group velocities of the pump and the forward propagating wave are matched, $v_p = v_s$. This gives a direct comparison between the two cases and shows that the nonlinear interactions in a BMOPO become more efficient in the case of exact group-velocity matching. Furthermore, the pump depletion (or the conversion efficiency) then also becomes rather insensitive to the spectral quality of the pump, due to the absence of temporal walk-off.

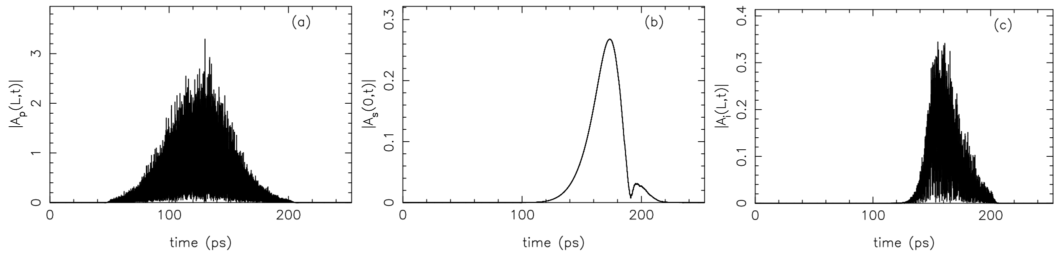

Fig. 15: Temporal evolution of the amplitudes in a BMOPO with the interacting wavelengths corresponding to exact group-velocity matching, pumped with stochastic phase modulated pulses and a bandwidth of $\Delta\nu_p = 23$ THz: (a) the forward pump, (b) the backward signal, and (c) the forward idler.

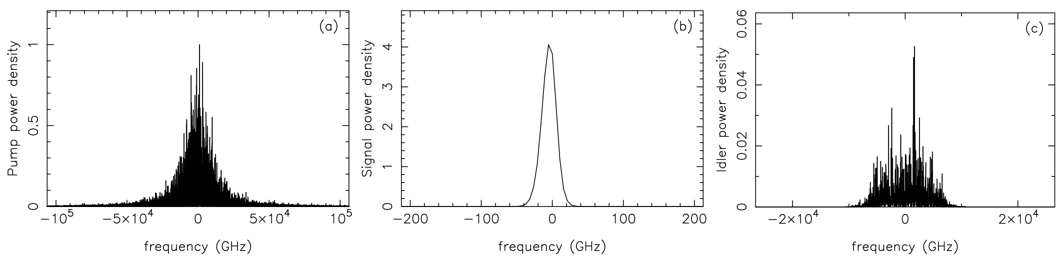

Fig. 16: (a) Incoherent pump spectrum with a bandwidth of $\Delta\nu_p = 23$ THz, (b) the backward signal spectrum with $\Delta\nu_s = 23$ GHz, (c) the forward idler spectrum with $\Delta\nu_i = 10$ THz. Coherence gain of 1000.

5.3 Incoherent pump pulse

One question that arises is if a BMOPO can operate when it is pumped with incoherent pulses. It is not obvious that such pulses can generate a spectrally-narrow backward-propagating parametric wave which is a characteristic feature of a BMOPO. In the conventional co-propagating configuration, the generation of a temporally coherent wave from a temporally incoherent pump has been numerically studied for i.e. parametric down-conversion [48] and has been experimentally verified for second-harmonic generation [49]. In order to answer the question in the counterpropagating BMOPO configuration, we used a pump pulse with randomly distributed phase variations, characterized by an exponential correlation function,

$$\left\langle \mathbf{A_p}(x=0,t'+t)\mathbf{A_p^*}(x=0,t)\right\rangle = \left|\mathbf{A_p}\right|^2 \exp\left(-|t|/\tau_c\right), \tag{20}$$

where $\tau_c = 1/\pi\Delta\nu_p$ is the correlation time. More precisely, we use a numerical scheme to generate a Gaussian spectrum with randomly-distributed phases and a small random variation in the amplitude, which simulates a real laser output where the amplitude exhibits small fluctuations over its Gaussian shape. In order to obtain a well-behaved Gaussian input, we impose a Gaussian profile on the Fourier spectrum and the pump amplitude is entered as the inverse Fourier transform.

As a result of the phase-locking mechanism, the transfer of phase modulation to the forward wave becomes more efficient when the group velocities of the pump and the forward parametric wave are exactly matched [39], which was already proposed for c.w. pumped forward OPO's [40] [42]. This was shown in Fig. 14. For z-polarized waves in PPKTP, matching of the group velocities can be achieved by designing the experiment so that the pump and the forward wave are on different sides of the maximum on the group-velocity curve: the singly backward wave may be now the signal, the co-propagating pump and idler waves satisfying $v_p = v_i$.

However, the combination of exact group-velocity matching and quasi-phase matching requires either a very short QPM period, which is hard to fabricate, or that the pump wavelength is substantially longer, which increases the BMOPO threshold. One example of a set of wavelengths that fulfill group-velocity matching are

$$\lambda_p = 1.0600\mu\text{m};\ n_p = 1.8298;\ v_p/c = 0.5341;\ \beta_p = 0.1752\ \text{ps}^2/\text{m}$$
$$\lambda_s = 1.6764\mu\text{m};\ n_s = 1.8129;\ v_s/c = 0.5405;\ \beta_s = 0.0290\ \text{ps}^2/\text{m}$$
$$\lambda_i = 2.8826\mu\text{m};\ n_i = 1.7826;\ v_i/c = 0.5341;\ \beta_i = -0.5784\ \text{ps}^2/\text{m}$$

where

$$\Lambda_{QPM} = \left[\frac{n_p}{\lambda_p} + \frac{n_s}{\lambda_s} - \frac{n_i}{\lambda_i}\right]^{-1} = 0.4567\ \mu\text{m}$$
$$\frac{\Delta v}{v_p} = \frac{|v_p - v_i}{v_p} = 0$$

We perform the numerical dynamics from equations (2) with $(-v_s, +v_i)$. Around the point of group-velocity matching, the BMOPO becomes more efficient and the spectral quality of the pump can be reduced without a large effect on the conversion efficiency. This is illustrated by running a simulation with a stochastic pump with a FWHM temporal length of 50 ps and where the spectral width is increased to 23 THz. At the pump intensity of 3.5 GW/cm^2, the results are shown in Fig. 15 and Fig. 16. The BMOPO starts oscillating after $t - t_0 = 60$ ps and the conversion efficiencies are $I_b(0)/I_p(0) = 0.025$ for the signal and $I_f(L)/I_p(0) = 0.015$ for the idler. Due to the group-velocity matching, the bandwidth of the backward signal is only 23 GHz. This value is significantly smaller than the bandwidth of backward wave in Fig. 16c, even though the pump bandwidth here has been increased by almost a factor of 6. In the case of group-velocity matching under the stated operational conditions, the spectral width of the backward-generated wave is reduced by a factor of 1000 compared to the width of the input pump spectrum. The random phase fluctuations in the pump are efficiently transferred to the forward idler, which obtains a spectral width of 10 THz.

For the experimental verification of BMOPO operation with an incoherent pump, a laser source is required that generates sub-ns pulses of energies around 100 μJ, at the same time as the pulses are incoherent. Good candidates for such a pump source are figure-eight fiber lasers operating in noise-like pulse mode with pulse lengths around 1 ns [50], which could be amplified to the required energies in fiber amplifiers.

5.4 Convection-induced phase-locking mechanism

The coherent properties of the parametric three-wave interaction driven from an incoherent pump has been the object of an analytical study where the autocorrelation functions are mathematically evaluated in the presence of dispersion [39] and the convection-induced phase-locking mechanism has been proposed for forward OPO's configurations [40] [42]. Let us present here some simple analytical arguments enlighting the convection-induced phase-locking mechanism from equations (2) for the singly backward signal configuration [case (c) of figure 1], Let us assume the dispersioless case ($\beta_j = 0$), $\sigma_s = \sigma_i = \sigma_p/2 = \sigma$, and the linear undepleted pump limit with $\gamma_p = 0$.

The incoherent pump may be modeled by a stationary single-variable stochastic function $A_p(z)$ of autocorrelation function

$$\frac{\langle A_p(z-z')A_p^*(z')\rangle}{|A_p(0)|^2} = \exp(-\frac{|z|}{\lambda_c})$$

with a coherence length λ_c in the frame traveling at its group velocity v_p,

$$z = x - v_p t,$$

the correlation time being $\tau_c \simeq 1/\pi\Delta\nu_p$, where $\Delta\nu_p$ is the incoherent (broad)-bandwidth of the pump spectrum. The role of convection in the coherence of the generated waves A_s and A_i may be analyzed by integrating the third equation (19) along the characteristic of the idler wave. Then, the second equation (19) yields

$$DA_s = \sigma^2 \int_0^t e^{-\gamma_i(t-t')} A_p(z)A_p^*(z')A_s(x',t')dt'$$

where

$$D = \partial/\partial t - v_s\partial/\partial x + \gamma_s$$

$$z' = z - (v_i - v_p)(t - t') \ ; \ \ x' = x - v_i(t - t')$$

If $v_i = v_p$ we have $z' = z$ and we can extract the pump amplitudes from the integral

$$A_p(z)A_p^*(z') = |A_p(z)|^2,$$

showing that the signal dynamics is independent of the pump phase fluctuations $\Phi_p(z)$.

This means that the rapid random phase fluctuations of the pump do not affect the signal which undergoes slow phase variations and thus evolves towards a highly coherent state during its parametric amplification.

Let us now consider the idler wave from the third equation (2):

$$A_i(x,t) = \sigma \int_0^t e^{-\gamma_i(t-t')} A_p(z')A_s^*(x',t')dt'.$$

When $v_i = v_p$ we have $z' = z$ and $A_p(z')$ becomes independent of t' which leads to an idler amplitude A_i proportional to the pump amplitude A_p *i.e.*, the idler field absorbs the noise of the co-moving pump field. Note that this *pump-idler phase-locking mechanism* does not require an exact matching of the group-velocities $v_i = v_p$. It is indeed sufficient that

$$|v_i - v_p| \ll \lambda_c\gamma_i = v_p t_c \gamma_i,$$

to remove the pump field from the integral so that the idler field follows the pump fluctuations. This phase-locking mechanisms may be demonstarted in realistic experimental configurations as studied in details in Ref.[39].

6 Summary

We have shown by a stability analysis of the non-degenerate backward OPO where both the signal and idler fields propagate backward with respect to the direction of the pump field that the inhomogeneous stationary solutions regularly bifurcate towards a time-dependent oscillatory solution contrarily to the degenerate case. We obtain a regular Hopf bifurcation for a critical

interaction length L_{crit}, which is finite only if a finite group velocity delay between the signal and the idler waves is taken into account.
This result has been confirmed by numerical simulations of the nonlinear dynamic equations, and an excellent agreement has been obtained near the degenerate configuration. Above L_{crit} self-structuration of symbiotic backward solitary waves - of some ps temporal duration - takes place. The finite temporal walk-off between the backscattered signal and idler waves also ensures the stability of the solitary waves. These short stable and coherent pulses could be very interesting for optical telecommunication. However, the susceptibility inversion grating of sub-μm period required for QPM in the nonlinear quadratic materials is still a technological challenge.

We have also considered mirrorless optical parametric oscillation in a PPKTP crystal, first by using linearly-chirped pump pulses with bandwidths of up to 4 THz in order to simulate recent experiments, and second by using highly incoherent pump pulses up to 23 THz bandwidth. It has been shown that the spectral bandwidth of the backward-generated pulse is more than two orders of magnitude narrower than that of the pump. In a general situation, the gain in temporal coherence of the backward-generated wave is limited by the group-velocity mismatch between the pump and the forward-generated wave. This mismatch also limits the conversion efficiency in the BMOPO. Numerically, we proved that the same conclusions are valid regardless of the nature of the phase modulation present in the pump wave by simulating operation of a BMOPO pumped by waves containing stochastic phase distributions. Moreover, we propose a generic BMOPO configuration where exact group-velocity matching can be achieved, thereby maximizing the gain in temporal coherence in the backward-propagating wave and making the efficiency of the device insensitive to the nature of the phase modulation present in the pump wave. This opens up an intriguing possibility for narrowband generation in MOPOs pumped with incoherent beams, e.g. derived from several lasers. Albeit the realization of such a MOPO requires QPM crystals which are slightly beyond the state-of-the-art of the current poling technology, the requirements are not unrealistic and can be met with the continuing development in fabrication techniques of submicrometer-periodicity nonlinear crystals. Improved fabrication techniques could also lead to the possibility of poling longer crystals. As the threshold intensity scales inversely to the square of the length of the structured region, an increase of this length from 6.5 mm to 18 mm results in a threshold intensity around 100 MW/cm^2, which is comparable to that in conventional co-propagating PPKTP OPOs.

7 Acknowledgments

The authors thank G. Strömqvist, V. Pasiskevicius and C. Canalias for stimulating discussions. They also acknowledge the GDR PhoNoMi2 n^o 3073 of the CNRS (Centre National de la Recherche Scientifique) devoted to Nonlinear Photonics in Microstructured Materials.

References

[1] J.A. Armstrong, S.S. Jha, and N.S. Shiren, IEEE J. Quant. Elect. **QE-6**, 123-129 (1970).

[2] K. Nozaki and T. Taniuti, J. Phys. Soc. Jpn. **34**, 796-800 (1973).

[3] D.J. Kaup, A. Reiman, and A. Bers, Rev. Mod. Phys. **51**, 275-309 (1979).

[4] K. Drühl, R.G. Wenzel, and J.L. Carlsten, Phys. Rev. Lett. **51**, 1171 (1983).

[5] S.L. McCall and E.L. Hahn, Phys. Rev. Lett. **18**, 908 (1967).

[6] S.C. Chiu, J. Math. Phys. **19** 168-176 (1978).

[7] C. Montes, A. Mikhailov, A. Picozzi, and F. Ginovart, Phys. Rev. E **55**, 1086-1091 (1997).

[8] C. Montes, A. Picozzi, and D. Bahlouol, Phys. Rev. E **55**, 1092-1105 (1997).

[9] E. Picholle, C. Montes, C. Leycuras, O. Legrand, and J. Botineau, Phys. Rev. Lett. **66**, 1454 (1991).

[10] C. Montes, A. Mamhoud, and E. Picholle, Phys. Rev. A **49**, 1344 (1994).

[11] C. Montes, D. Bahloul, I. Bongrand, J. Botineau, G. Cheval, A. Mamhoud, E. Picholle, and A. Picozzi, J. Opt. Soc. Am. B **16**, 932 (1999).

[12] J. Botineau, G. Cheval, and C. Montes, Opt. Commun. **257**, 319-33 (2006).

[13] C. Montes *Dissipative Solitons : From Optics to Biology and Medecine* (N. Akhmediev and A. Ankiewicz, Springer-Verlag, Lecture Notes in Physics **751**, Berlin) 221-260 (2008).

[14] A. Picozzi and M. Hælterman, Opt. Lett. **23**, 1808 (1998).

[15] A. Picozzi and M. Haelterman, Phys. Rev. Lett. **84**, 5760-5762 (2000).

[16] C. Montes, A. Picozzi, and M. Hælterman, *Optical Solitons: Theoretical Challenges and Industrial Perspectives* Les Houches Workshop sep.28-oct.2 1998, (V.E. Zakharov and S. Wabnitz, EDP Springer), 283-292 (1999).

[17] C. Montes, *Optical Solitons : Theory and Experiments* (K. Porsezian and V.C. Kuriakos, Springer-Verlag, Berlin), 353-371 (2003).

[18] C. Durniak, C. Montes and M. Taki, J.Opt. B: Quantum Semiclass. Opt. **6**, S241-S249 (2004).

[19] C. Montes, A. Picozzi, C. Durniak, and M. Taki, Eur. Phys. J. Special Topics **173**, 167-191 (2009).

[20] M. Matsumoto and K. Tanaka, IEEE J. Quantum Electron. **31**, 700 (1995).

[21] Y.J. Ding and J.B. Khurgin, IEEE J. Quantum Electron. **32**, 1574-1582 (1996).

[22] J.U. Kang, Y.J. Ding, W.K. Burns, and J.S. Melinger, Opt. Lett. **22**, 862 (1997).

[23] G. D'Alessandro, P.St. Russell, and A.A. Wheeler, Phys. Rev. A **55**, 3211 (1997).

[24] C. Canalias and V. Pasiskevicius, Nature Photonics, **1**, 459-462 (2007).

[25] G. Strömqvist, V. Pasiskevicius, C. Canalias, and C. Montes, Phys. Rev. A **84**, 023845-1-4 (2011).

[26] G. Strömqvist, V. Pasiskevicius, C. Canalias, P. Aschieri, A. Picozzi, and C. Montes, J. Opt. Soc. Am. B (2012)

[27] A. Picozzi and M. Hælterman, Phys. Rev. Lett.,**86**, 2010 (2001).

[28] C. Montes, C. Durniak, M. Taki, and A. Picozzi, Opt. Commun. **216**, 419-426 (2003).

[29] S.F. Morozov, L.V. Piskunova, M.M. Sushchik, and G.I. Freidman, Sov. J. Quant. Electron. **8**, 576 (1978).

[30] A.D.D. Craik, M. Nagata, and I.M. Moroz, Wave Motion **15**, 173 (1992).

[31] J.A. Armstrong, N. Bloembergen, J. Ducuing, and N. Pershan, Phys. Rev. **127** 1918-1939 (1962).

[32] A.C. Busacca, C.L. Sones, R.W. Eason, and S. Mailis, Applied Phys. Lett. **84**, 4430-4432 (2004).

[33] V.G.Dmitriev, G.G. Gurzadyan, D.N. Nikogosyan, *Handbook of Nonlinear Optical Crystals* (Springer-Verlag, Berlin, 74 for $LiNbO_3$ and 103 for $KTiOPO_4$ (1991).

[34] G.P. Bava, I. Montrosset, W. Sohler, and H. Suche, IEEE J. Quantum Electron. **QE-23**, 42 (1987).

[35] H. Suche and W. Sohler, *Integrated optical parametric oscillators* (invited), Optoelectronics-Devices and Technologies, Japan, **4**(1), 1-20 (1989).

[36] M.A. Arbore and M.M. Fejer, Opt. Lett. **22**, 151-153 (1997).

[37] D. Hofmann, H. Herrmann, G. Schreiber, W. Grundkötter, R. Ricken, and W. Sohler, *Continuous-wave mid-infrared optical parametric oscillators with periodically poled Ti:*$LiNbO_3$ *waveguide*, in *9th European Conference on Integrated Optics and Technical Exhibition* ECIO'99 (EOS - European Optical Society) p. 21 (1999).

[38] D. Hofmann, H. Herrmann, G. Schreiber, C. Haase, W. Grundkötter, R. Ricken, and W. Sohler, in *Nonlinear Guided Waves and Their Applications* (Optical Society of America, Washington, D.C.), FC2-1-3, p.465 (1999).

[39] A. Picozzi, C. Montes, and M. Hælterman, Phys. Rev E **66**, 056605-1-14 (2002).

[40] C. Montes, A. Picozzi, and K. Gallo, Opt. Commun. **237**, 437-449 (2004).

[41] A. Picozzi and P. Aschieri, Phys. Rev. E **72**, 046606-1-12 (2005).

[42] C. Montes, W. Grundkötter, H. Suche, and W. Sohler, J. Opt. Soc. Am. **24** 112796-11280 (2007).

[43] S.E. Harris, Appl. Phys. Lett. **9**, 114 (1966).

[44] W. Shi and Y.J. Ding, Optics Lett. **30**, 1861-1863 (2005).

[45] S.P. Smith, F. Zarinetchi, and S. Ezekiel, Opt. Lett. **16**, 393-395 (1991)

[46] K. Kato and E. Takaoka, Appl. Opt., **41**, 5040, (2002).

[47] C. Montes, P. Aschieri, and A. Picozzi, SPIE Proc. **8011**, 801136-1-10 (2011).

[48] A. Piskarskas, V. Pyragaite, and A. Stabinis, Phys. Rev. A **82**, 053817 (2010).

[49] A. Stabinis, V. Pyragaite, G. Tamošauskas, and A. Piskarskas, Phys. Rev. A **84**, 043813 (2011).

[50] K. Özgören, B. Öktem, S. Yilmaz, F.Ö. Ilday and Koray Eken, Opt. Express **18**, 17647-17652 (2011).